

Crystalline orthorhombic Ln[CO₃][OH] (Ln=La, Pr, Nd, Sm, Eu, Gd) compounds hydrothermally synthesised with CO₂ from air as carbonate source

Matthias Hämmer, Henning A. Höppe

Angaben zur Veröffentlichung / Publication details:

Hämmer, Matthias, and Henning A. Höppe. 2019. "Crystalline orthorhombic Ln[CO₃][OH] (Ln=La, Pr, Nd, Sm, Eu, Gd) compounds hydrothermally synthesised with CO₂ from air as carbonate source." Zeitschrift für Naturforschung B 74 (1): 59-70. <https://doi.org/10.1515/znb-2018-0170>.



Matthias Hämmer and Henning A. Höpfe*

Crystalline orthorhombic $Ln[CO_3][OH]$ ($Ln = La, Pr, Nd, Sm, Eu, Gd$) compounds hydrothermally synthesised with CO_2 from air as carbonate source

<https://doi.org/10.1515/znb-2018-0170>

Received August 15, 2018; accepted October 26, 2018

Abstract: Crystalline orthorhombic rare earth carbonate hydroxides $Ln[CO_3][OH]$ ($Ln = La, Pr, Nd, Sm, Eu, Gd$) were synthesised as phase pure powders via a simple hydrothermal reaction. CO_2 from air acted as natural carbonate source and cetyltrimethylammonium bromide was added as templating agent to an aqueous rare earth nitrate solution. Single-crystal X-ray structure determination was performed on $La[CO_3][OH]$ ($Pnma$, $a = 7.4106(5)$, $b = 5.0502(3)$, $c = 8.5901(6)$ Å, 563 independent reflections, 38 refined parameters, $wR2 = 0.037$), $Pr[CO_3][OH]$ ($Pnma$, $a = 7.2755(4)$, $b = 4.9918(3)$, $c = 8.5207(5)$ Å, 744 independent reflections, 38 refined parameters, $wR2 = 0.04$), $Eu[CO_3][OH]$ ($Pnma$, $a = 7.1040(4)$, $b = 4.8940(3)$, $c = 8.4577(5)$ Å, 1649 independent reflections, 38 refined parameters, $wR2 = 0.05$) and $Gd[CO_3][OH]$ ($Pnma$, $a = 7.069(7)$, $b = 4.874(5)$, $c = 8.464(9)$ Å, 431 independent reflections, 38 refined parameters, $wR2 = 0.051$). These findings are supported by powder XRD, infrared spectroscopy, UV/Vis spectroscopy and, for $Pr[CO_3][OH]$ and $Eu[CO_3][OH]$, by measurements of the non-linear optical properties. Thermal analysis could demonstrate the possible use of the $Ln[CO_3][OH]$ phases as precursors for rare earth carbonate dioxides $Ln_2[CO_3]O_2$ and rare earth oxides Ln_2O_3 . The decomposition products inherit the precursor's morphology. The lattice parameters of $Pr_2[CO_3]O_2$ were refined from high-temperature powder XRD data.

Keywords: carbonate; crystal structure; hydroxides; lanthanide; precursor.

Dedicated to: Professor Wolfgang Bensch on the Occasion of his 65th birthday.

*Corresponding author: Henning A. Höpfe, Lehrstuhl für Festkörperchemie, Institut für Physik, Universität Augsburg, Universitätsstraße 1, 86159 Augsburg, Germany, e-mail: henning@ak-hoeppe.de.
<https://orcid.org/0000-0002-8734-8258>

Matthias Hämmer: Lehrstuhl für Festkörperchemie, Institut für Physik, Universität Augsburg, Universitätsstraße 1, 86159 Augsburg, Germany. <https://orcid.org/0000-0003-0056-0959>

1 Introduction

In the course of our systematic investigation on silicate-analogous materials [1–5] we also try to identify suitable precursor compounds. In this context we came across the rare earth carbonate hydroxides $Ln[CO_3][OH]$, a highly interesting class of materials with promising applications as host materials for phosphors [6, 7], catalysts [8], magnetic-cooling materials [9], and precursors for both rare earth carbonate dioxides and rare earth oxides and further synthesis. A selection of contributions is found in refs. [7, 10–17]. The rare earth carbonate dioxides $Ln_2[CO_3]O_2$ can be used also as catalysts or catalyst support [18], as host materials for luminescent applications [6, 7, 19, 20] and as precursors for further syntheses [10, 21]. The pure rare earth oxides Ln_2O_3 are well known as host materials for phosphors [16, 19, 22]. The use of cheap and readily available precursors is most attractive if the morphology of the product is similar to that of the precursor [12–14, 23].

In general, rare earth carbonate hydroxides occur in three modifications: A hexagonal modification crystallising in space group $P\bar{6}$, an orthorhombic modification and a tetragonal modification crystallising in space group $P4_2/nmc$ only for Tm and Yb [13, 24–28]. The orthorhombic polymorph is reported in space group $Pnma$ for the large rare earth ions Pr, Nd and Sm. For smaller rare earth ions than Sm (Eu, Gd, Tb, Dy, Ho, Er, Tm and Y) space group $P2_12_12_1$ can be found in the literature [13, 24, 26, 28, 29]. Nevertheless, space group $Pnma$ is also reported for $Gd[CO_3][OH]$ [9, 30] showing disagreement with the exact structure of the orthorhombic modification.

Several syntheses for rare earth carbonate hydroxides are reported in literature via homogeneous precipitation [7, 11, 13, 16], hydrothermal methods [6, 8, 13, 15, 17, 24, 27, 31], solvothermal methods [32], and thermolysis [10].

In nature, the mineral *ancylite* $La_2O(CO_3)_2 \cdot H_2O$ crystallises in space group $Pnma$ [33]. It is the only rare earth oxycarbonate hydrate for which the crystal structure has been solved [13, 33]. Dal Negro et al. solved the structure using a single crystal from geological origin [33]. We show here that this compound is isotypic with orthorhombic $La[CO_3][OH]$ [24]. This implies that this rare

earth oxycarbonate hydrate is truly a rare earth carbonate hydroxide in the orthorhombic modification. Chemical intuition points into the same direction since the structure reported by Dal Negro et al. lacks any oxygen atom not being part of the carbonate ion or the proposed water molecule [33]. The same presumably holds true for the relationship of the minerals *kozoite* $Nd[CO_3][OH]$ and $La[CO_3][OH]$ plus *calcioancylite* $CeCa(CO_3)_2(OH) \cdot H_2O$ with their respective carbonate hydroxides [34–36].

In general, there are three modifications of $Ln_2[CO_3]O_2$, the thermal decomposition product of $Ln[CO_3][OH]$. Crystallographically closely related are the orthorhombic (“type-I”, space group $Ama2$) and monoclinic (“type-Ia”, space group $C2/c$) polymorphs only described so far for La, while the hexagonal (“type-II”, space group $P6_3/mmc$) one is found for La, Nd, Gd and Dy [13, 30, 37–40].

In this contribution, we present the hydrothermal synthesis of orthorhombic $Ln[CO_3][OH]$ ($Ln = La, Pr, Nd, Sm, Eu, Gd$) using CO_2 from air as carbonate source. This process is likely to resemble the pathway followed in nature to form minerals such as *ancylite* or *kozoite* giving further insight into the formation of these minerals [33–35].

The crystal structures of $Pr[CO_3][OH]$, $Eu[CO_3][OH]$ and $Gd[CO_3][OH]$ are redetermined localising also the hydrogen atoms, and the first report on the structure of orthorhombic $La[CO_3][OH]$ based on single-crystal XRD data is given. We elucidated the structures with a special focus on the presence or absence of inversion symmetry as this point was under discussion in the literature. Further, the use of the materials as precursors for $Ln_2[CO_3]O_2$ and Ln_2O_3 is demonstrated. The lattice parameters of $Pr_2[CO_3]O_2$ have been refined by high-temperature powder XRD analysis.

2 Results and discussion

2.1 Syntheses

Phase-pure samples of $Ln[CO_3][OH]$ ($Ln = La, Pr, Nd, Sm, Eu, Gd$) were obtained via a facile hydrothermal process starting from aqueous solutions of $Ln(NO_3)_3 \cdot xH_2O$ (Fig. 1 and Fig. S1; Supporting Information available online). Cetyltrimethylammonium bromide (CTAB) was added. It is well known to serve as a templating agent [13, 23]. In literature, comparable syntheses using $CO(NH_2)_2$, Na_2CO_3 , $NaHCO_3$, $(NH_4)_2CO_3$ and others as carbonate sources have been reported [13, 15, 31]. CO_2 is thought to

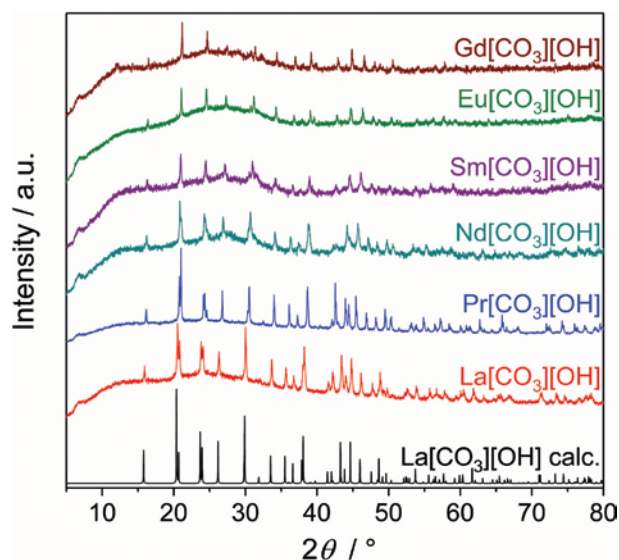


Fig. 1: Powder XRD patterns of compounds $Ln[CO_3][OH]$ ($Ln = La, Pr, Nd, Sm, Eu, Gd$) compared to a pattern calculated from single-crystal data of $La[CO_3][OH]$. All calculated patterns of the determined structures can be found in Fig. S1 (Supporting Information).

act as carbonate source in the solvothermal synthesis of hexagonal $La[CO_3][OH]$ in an ionic liquid-water mixture [32]. Accordingly, we report the first intended hydrothermal synthesis using only CO_2 from ambient air as carbonate source and we further demonstrate how easily these compounds are formed.

All syntheses yielded homogeneous, coarsely crystalline products $Ln[CO_3][OH]$ ($Ln = La, Pr, Nd, Sm, Eu, Gd$). The CTAB apparently has an influence on particle sizes and shape distributions (Fig. S2; Supporting Information). For $Ln = Nd, Sm, Eu$ and Gd an additional heating step at $350^\circ C$ was necessary to decompose residual CTAB and an unknown side product. The presence of these side phases was shown by infrared spectroscopy (Fig. S3; Supporting Information), their decomposition around $350^\circ C$ could be followed by DSC measurements (Fig. S4; Supporting Information); this thermal behavior of CTAB is well known [41].

Surprisingly, the use of $Ce(NO_3)_3 \cdot 5H_2O$ yielded phase-pure CeO_2 single crystals (Fig. S5, Supporting information). Similar syntheses also using CTAB as templating ligand are known in the literature [42]. The reason for this behaviour can be found in the high stability of CeO_2 at low oxygen partial pressures [43].

In the context addressed in the introduction we performed single-crystal X-ray structure determinations on $La[CO_3][OH]$, $Pr[CO_3][OH]$, $Eu[CO_3][OH]$ and $Gd[CO_3][OH]$ (Table 1), accompanied by optical and thermal characterisation of these compounds.

Table 1: Crystal data and structure refinements of $La[CO_3][OH]$, $Pr[CO_3][OH]$, $Eu[CO_3][OH]$ and $Gd[CO_3][OH]$ ^a.

	$La[CO_3][OH]$	$Pr[CO_3][OH]$	$Eu[CO_3][OH]$	$Eu[CO_3][OH]$	$Gd[CO_3][OH]$
$M/g\ mol^{-1}$	215.93	217.93	228.98	228.98	234.27
Crystal size/mm ³	$0.02 \times 0.06 \times 0.06$	$0.04 \times 0.06 \times 0.10$	$0.05 \times 0.05 \times 0.13$	$0.05 \times 0.05 \times 0.13$	$0.03 \times 0.04 \times 0.06$
Temperature/K			300(2)		
Space group	$Pnma$ (No. 62)	$Pnma$ (No. 62)	$Pnma$ (No. 62)	$P2_12_12_1$ (No. 19)	$Pnma$ (No. 62)
a/pm	741.06(5)	727.55(4)	710.40(4)	710.40(4)	706.9(7)
b/pm	505.02(3)	499.18(3)	489.40(3)	489.40(3)	487.4(5)
c/pm	859.01(6)	852.07(5)	845.77(5)	845.77(5)	846.4(9)
Volume/ $10^6\ pm^3$	321.48(4)	309.45(3)	294.05(3)	294.05(3)	291.7(5)
Z			4		
$\rho_{\text{calc}}/g\ cm^{-3}$	4.46	4.68	5.17	5.17	5.34
Absorption coefficient μ/mm^{-1}	13.1	15.6	21.1	21.1	22.6
$F(000)/e$	384	392	408	408	412
Radiation; wavelength $\lambda/\text{\AA}$			MoK α ; 0.71073		
Diffractometer			Bruker D8 Venture		
Absorption correction			Multi-scan		
Transmission (min; max)	0.5936; 0.7461	0.6578; 0.7474	0.5307; 0.7503	0.5307; 0.7503	0.5815; 0.7465
Index range $h\ k\ l$	$-10/10\ -6/7\ -12/12$	$-10/12\ -8/8\ -13/14$	$-15/15\ -10/10\ -15/18$	$-15/15\ -10/10\ -15/18$	$-9/9\ -6/6\ -11/11$
θ range/deg	3.631–30.964	3.682–35.988	3.746–49.967	3.746–49.967	3.755–29.917
Reflections collected	3558	6776	8923	9324	3121
Independent reflections	563	801	1649	3076	465
R_{int}	0.0320	0.0469	0.0312	0.0292	0.073
Obs. reflections ($> 2\ \sigma(I)$)	492	676	1478	2600	386
Refined parameters	38	38	38	61	38
R_1 (all data)	0.0238	0.0298	0.0291	0.0290	0.0412
wR_2 (all data)	0.0369	0.0409	0.0502	0.0438	0.0524
Goof	1.118	1.094	1.347	1.091	1.081
Flack x parameter	–	–	–	0.59(5) (refined as an inversion twin)	–
Residual electron density (max; min)/ $e^{-\text{\AA}^{-3}}$	1.35; –0.96	1.74; –1.22	2.77; –2.25	2.54; –1.37	1.26; –1.28

^aThe respective standard deviations are given in parentheses.

2.2 Crystal structures

2.2.1 $Ln[CO_3][OH]$ ($Ln = La, Pr, Eu, Gd$)

All four compounds crystallise isotypically with *kozoite* in space group $Pnma$ [24]. Five carbonate and two hydroxide groups are coordinated to the respective Ln^{3+} ion. Two carbonate groups act as monodentate and three as chelate ligands. Thus, the Ln^{3+} ions are coordinated by ten oxygen atoms (Fig. 2). The Ln^{3+} cation and the OH^- groups form ${}^1_2[(OH)Ln_{2/2}]^{2+}$ zigzag chains along $[100]$ linked by carbonate anions [24]. The OH^- anions are oriented towards the resulting channels between the chains (Fig. 3). Each carbonate group acts as a chelate ligand to three Ln^{3+} ions and as a monodentate ligand to two other Ln^{3+} ions. Consequently, the carbon centre is coordinated by three oxygen atoms in the first and surrounded by five Ln^{3+} ions in the second coordination sphere.

The Ln^{3+} cations are situated on Wyckoff site $4c$ with the $Ln-O$ distances ranging from 240–278 pm ($La[CO_3][OH]$), 236–276 pm ($Pr[CO_3][OH]$), 230–275 pm ($Eu[CO_3][OH]$), and 230–276 pm ($Gd[CO_3][OH]$) (Table 2). These values are reasonably close to the sum of the respective ionic radii [44]. The distances between adjacent Ln^{3+} ions are decreasing, following the lanthanide contraction, and the $Ln-O$ distances follow the same trend. The bond lengths within the carbonate ions are below the sum of the ionic radii of 130 pm [44] implying a covalent bond. The $O-C-O$ angles are close to 120° . $Gd[CO_3][OH]$ has the largest deviation due to the increased repulsion between carbonate groups since their distance is decreasing with the lanthanide contraction.

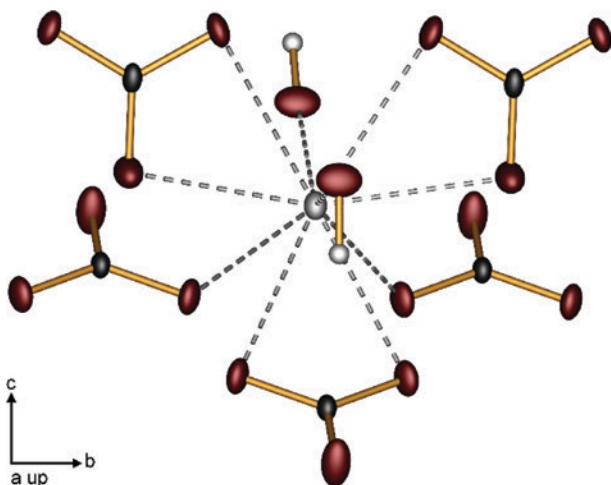


Fig. 2: Coordination of the Ln^{3+} cation in $Ln[CO_3][OH]$ in space group $Pnma$ (grey: Ln , black: C, white: H, red: O); displacement ellipsoids are set to 75% probability.

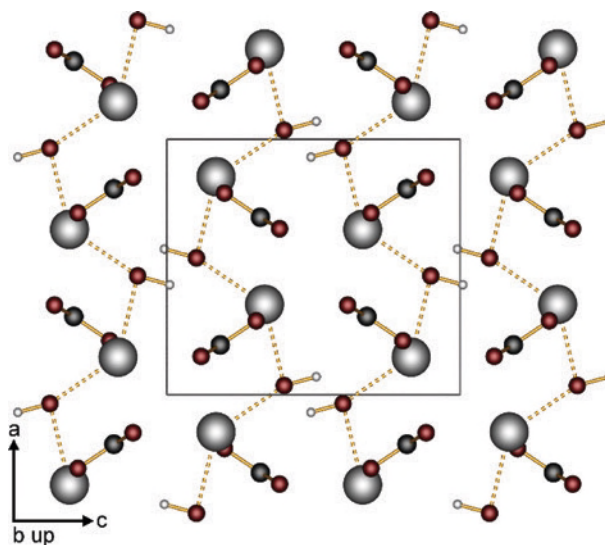


Fig. 3: ${}^1_2[(OH)Ln_{2/2}]^{2+}$ zigzag chains along $[100]$ with OH^- groups oriented towards the resulting channels in $Ln[CO_3][OH]$ (grey: Ln , black: C, white: H, red: O).

Evaluation of the literature yields two main aspects under discussion regarding “ $LnCO_4H$ ”, a chemical and a crystallographic one.

The crystal structure of $La[CO_3][OH]$ ($Pnma$, $Z=4$) appears to be isostructural to *ancylite* $La_2O(CO_3)_2 \cdot H_2O$ ($Pnma$, $Z=2$) [24]. Our data suggest that they are actually isotypic. The only difference is the presence of OH^- anions or H_2O molecules besides O^{2-} ions; from a chemical point of view the latter discrimination is only reasonable if both oxygen atoms find themselves in different chemical environments, otherwise a simple acid base reaction yielding to hydroxide ions can take place. Both, the chemical environment and our electrostatic calculations (see below) suggest the presence of two hydroxide ions instead of water molecules besides oxide ions. A similar behaviour is reported for $Gd[CO_3][OH]$ and $Gd_2O(CO_3)_2 \cdot H_2O$ [9]. The structure model presented by dal Negro et al. contains only crystal water and no oxide [33]; this disagrees with an overall electrostatically neutral formula. The assumption that the structure is that of a hydrate is not in agreement with the high thermal stability of the material [9]. The first decomposition step takes place above $400^\circ C$ [11–15, 31]. For crystal water, a loss at lower temperatures is expected [45]. We therefore conclude that the structure is indeed a carbonate hydroxide, and we were indeed able to localise the hydrogen atom during the structure refinement. Consequently, all reported syntheses for $Ln_2O(CO_3)_2 \cdot H_2O$ using the analogy to *ancylite* can be taken as routes to orthorhombic $Ln[CO_3][OH]$ compounds [9, 11, 13].

The same holds for the refined crystal structure of $Pr[CO_3][OH]$ which thus agrees well with Heinrich’s

Table 2: Selected interatomic distances (in pm) and angles (in deg) of $La[CO_3][OH]$, $Pr[CO_3][OH]$, $Eu[CO_3][OH]$ and $Gd[CO_3][OH]^a$.

	$La[CO_3][OH]$	$Pr[CO_3][OH]$	$Eu[CO_3][OH]$	$Gd[CO_3][OH]$
$Ln-O_c^b$	258.13(8)–278.0(2)	255.06(7)–275.5(2)	250.30(5)–274.89(17)	249.7(3)–275.8(5)
$Ln-O_H^c$	240.9(3)–242.7(3)	236.2(3)–237.2(3)	230.4(2)–231.0(2)	229.8(7)–230.4(7)
$\Sigma IR(Ln-O)$ [44] ^d	263; 265	254; 256	248; 250	247; 249
$Ln-Ln$	396.85(4)	390.45(4)	382.89(3)	381.54(34)
C–O	126.5(5)–129.4(3)	126.7(5)–129.1(3)	126.9(3)–128.6(2)	124.4(12)–129.3(7)
C–C	388.67(63)	382.73(61)	376.61(40)	374.82(119)
O–C–O	119.3(4)–120.31(18)	119.7(3)–120.05(17)	119.3(2)–120.29(12)	117.7(8)–121.1(4)
O–Ln–O	49.28(9)–94.45(5)	49.19(8)–94.84(5)	49.64(6)–95.08(4)	49.43(17)–94.83(11)

^aThe respective standard deviations are given in parentheses; ^b O_c = oxygen as part of the carbonate group; ^c O_H = oxygen as part of the hydroxide group; ^d Different sums of ionic radii due to oxygen with both CN = 3 and 4.

Rietveld refinement [28]. Also in this case we were able to localise the hydrogen atoms.

Another aspect of the discussion regarding the proper structure model is the presence or absence of an inversion centre, i.e. space group $P2_12_12_1$ vs. $Pnma$. Tahara et al. reported $Eu[CO_3][OH]$ in $P2_12_12_1$, while we refined the structure without any peculiarities in space group $Pnma$ [24]. There is a similar disagreement over the structure of $Gd[CO_3][OH]$, which was reported in both space groups [9, 24, 30]. Both solutions differ in the lack of centrosymmetry of space group $P2_12_12_1$ resulting in a postulated change of the coordination sphere of the Eu^{3+} ion – not really justified by a close look on the interatomic distances and MAPLE calculations (Tables S1 and S2; Supporting Information). Three carbonate groups are monodentate ligands and only two are chelating ligands in this described solution, because the carbonate group lost its symmetry from C_{2v} to C_s [7, 46, 47]. This modification is explained by the increased repulsion between the CO_3^{2-} anions due to the smaller ionic radius of Eu^{3+} following the lanthanide contraction [24]. This structure in space group $P2_12_12_1$ was first reported for $Y[CO_3][OH]$ [29].

The refinement of the single-crystal X-ray data implies unambiguously a centrosymmetry due to similar residuals. Possible explanations are a centrosymmetric space group or an inversion twin. The space group $Pnma$ was confirmed using the program PLATON [48]. Non-centrosymmetric crystal structures necessarily show non-linear optical properties – normally proven by recording the SHG (second harmonic generation) intensity [49]. We used the powder SHG method developed by Kurtz and Perry [50]. Table S3 (Supporting Information) shows the intensity of the SHG signals and comparisons to the quartz reference. In the cases of both $Pr[CO_3][OH]$ and $Eu[CO_3][OH]$ no respective signal could be detected in very careful measurements, thus apparently both structures are centrosymmetric. The same consideration holds for $Gd[CO_3][OH]$. Structure determinations have been reported

in both $Pnma$ and $P2_12_12_1$ [9, 24, 30]. Using the new data, the structure could only reliably be solved and refined in space group $Pnma$ (Table 1).

2.2.2 $Ln_2[CO_3]O_2$

The lattice parameters of the intermediate product $Pr_2[CO_3]O_2$ ($a = 4.0388$, $c = 15.7651$ Å) could be determined using a high-temperature powder XRD measurement at 720°C (Fig. S6; Supporting Information) with the crystal structure of $La_2[CO_3]O_2$ ($a = 4.0755$, $c = 15.957$ Å, space group $P6_3/mmc$ (No. 194)) [37] as a model. The refinement based on the CIF data of the lanthanum compound [37] was carried out using the program JANA2006; $R_1 = 7.11$, $R_2 = 6.40$, $GooF = 1.05$ [51]. The refined lattice parameters are in agreement with the reported structures of $Nd_2[CO_3]O_2$, $Gd_2[CO_3]O_2$ and $Dy_2[CO_3]O_2$ taking into account the lanthanide contraction [30, 39, 40]. The synthesis of $Pr_2[CO_3]O_2$ was achieved via thermolysis of $Pr(O_2C_2H_3)_3$, but no structure has been reported in literature [10].

As already discussed in the introduction, the structure of hexagonal Type II $Ln_2[CO_3]O_2$ has been refined in space group $P6_3/mmc$. $[OLn_4]$ tetrahedra are connected via edges to form layers parallel (001). These layers are stacked along [001] with layers of CO_3^{2-} ions, leading to the overall formula $(LnO)_2(CO_3)$. The carbonate groups are disordered around [001], the C position and one O position being only 1/3 occupied; which does not appear to make sense. The Ln^{3+} ion is coordinated by four oxygen atoms from the CO_3^{2-} groups and four naked O^{2-} [39].

Nevertheless, the facts that the C position and one O position are disordered with an occupation factor of 1/3 and the ratio of a/c is roughly 1/3 in space group $P6_3/mmc$ strongly imply that there is an underlying lower symmetry in a primitive orthorhombic space group, in which the carbonate ions are not disordered. Similar findings for $Gd_4[BO_2]O_5F$ have been reported in literature [52].

However, this investigation is beyond the scope of the present contribution.

2.3 Electrostatic calculations

The electrostatic reasonability of the crystal structures was confirmed by calculations based on the MAPLE concept (MAdelung Part of Lattice Energy) [53–55]. The MAPLE

Table 3: Electrostatic calculations for the rare earth carbonate hydroxides $Ln[CO_3][OH]$ ($Ln = La, Pr, Eu, Gd$) in space group $Pnma$.

La[CO ₃][OH]	$\frac{1}{2} La_2O_3$ [56] + H ₂ O [57] + CaCO ₃ [58] – CaO [59]
MAPLE = 27 016 kJ mol ⁻¹	MAPLE = 27 084 kJ mol ⁻¹ ($\Delta = 0.25\%$)
Pr[CO ₃][OH]	$\frac{1}{2} Pr_2O_3$ [60] + H ₂ O [57] + CaCO ₃ [58] – CaO [59]
MAPLE = 27 336 kJ mol ⁻¹	MAPLE = 27 201 kJ mol ⁻¹ ($\Delta = 0.49\%$)
Eu[CO ₃][OH]	$\frac{1}{2} Eu_2O_3$ [61] + H ₂ O [57] + CaCO ₃ [58] – CaO [59]
MAPLE = 27 520 kJ mol ⁻¹	MAPLE = 27 448 kJ mol ⁻¹ ($\Delta = 0.26\%$)
Gd[CO ₃][OH]	$\frac{1}{2} Gd_2O_3$ [61] + H ₂ O [57] + CaCO ₃ [58] – CaO [59]
MAPLE = 27 571 kJ mol ⁻¹	MAPLE = 27 483 kJ mol ⁻¹ ($\Delta = 0.32\%$)

Table 4: EDX results for $Ln[CO_3][OH]$ ($Ln = La, Pr, Eu, Gd$) comparing the ratio of Ln to O to the stoichiometric value of 0.25^a.

Sample	EDX result
La[CO ₃][OH]	0.19(5)
Pr[CO ₃][OH]	0.18(3)
Eu[CO ₃][OH]	0.27(6)
Gd[CO ₃][OH]	0.26(6)

^aThe respective standard deviations are given in parentheses.

values of La[CO₃][OH], Pr[CO₃][OH], Eu[CO₃][OH] and Gd[CO₃][OH] were calculated and compared to the sum of the respective chemically comparable rare earth oxides, ice and a hypothetical CO₂ derived from the difference of CaCO₃ and CaO (Table 3) – an approach also employed recently for other oxides, in which the respective crystal structure comprises only molecules [62]. For CaCO₃, the aragonite structure was chosen since its carbonate group shows C_s symmetry being close to the C_{2v} symmetry of the carbonate groups in the present compounds [47]. The deviation is well below 1% for all four structures, which is our empirical benchmark for electrostatic consistency. The MAPLE values for Eu[CO₃][OH] in space groups $Pnma$ and $P2_12_12_1$ do not differ significantly (Table S4; Supporting Information).

2.4 SEM and EDX investigations

The $Ln[CO_3][OH]$ ($Ln = La, Pr, Eu, Gd$) samples were investigated by EDX. The results shown in Table 4 match well with the expected ratios of the respective rare earth element and oxygen. The simultaneously taken SEM pictures show the crystallinity of the compound (See Fig. 4).

2.5 Infrared spectroscopy

Infrared spectroscopy was performed on the phase pure powders of the $Ln[CO_3][OH]$ compounds ($Ln = La, Pr, Nd, Sm, Eu, Gd$). The spectra shown in Fig. 5 fit to structural units of the determined structures and to reports in literature for related systems [6–8, 14, 31].

The OH stretching and bending vibrations appear around 3440 cm⁻¹, between 1680 and 1630 cm⁻¹ and around 1320 cm⁻¹ [6, 7, 12]. In agreement with the O–H···O distance derived from single-crystal structure determination, the second mode is shifted from La[CO₃][OH] to

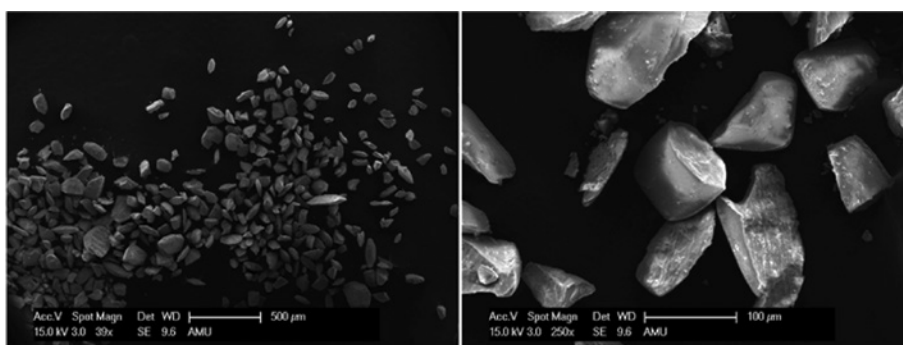


Fig. 4: SEM pictures of as prepared La[CO₃][OH] taken simultaneously to the EDX measurement.

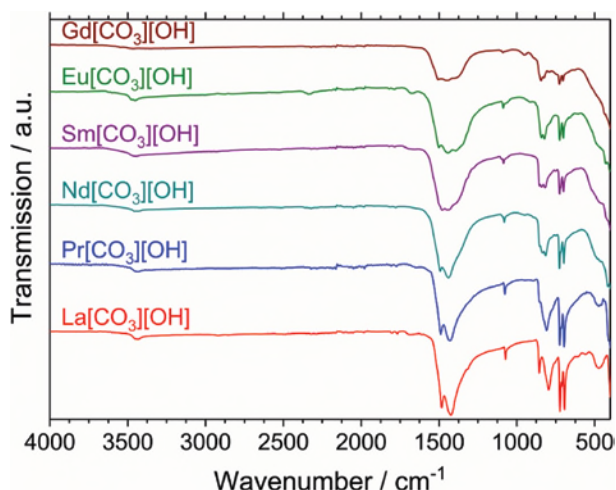


Fig. 5: Infrared spectra of $Ln[CO_3][OH]$ ($Ln = La, Pr, Nd, Sm, Eu, Gd$).

$Gd[CO_3][OH]$ to higher wavenumbers [47, 63]. The products are free of the starting material CTAB since the expected absorption bands $\nu_{as}(C-CH_2)$ and $\nu_s(C-CH_2)$ at 2920 and 2850 cm^{-1} are absent [23]. The bands between 1500 and 600 cm^{-1} can be assigned to coordinated CO_3^{2-} . The four normal modes can be found at 1090–1070 cm^{-1} (ν_1), 850–840 cm^{-1} (ν_2), 1500–1480 cm^{-1} and 1440–1420 cm^{-1} (ν_3) plus 725 cm^{-1} and 700–690 cm^{-1} (ν_4) [6, 7, 12]. The splitting of the degenerated modes ν_3 and ν_4 is caused by the symmetry reduction from D_3 to C_{2v} or C_s from the free to the coordinated carbonate anion (Table 5) [6, 7, 12, 46, 47]. For $Eu[CO_3][OH]$, a discrimination between both possible space groups $Pnma$ and $P2_12_12_1$ corresponding to the CO_3^{2-} ion's point group C_{2v} and C_s is not possible based on the IR spectrum since six IR-active bands are expected for both symmetries compared to only three for both higher symmetries D_{3h} and D_3 . Additionally, the CO_3^{2-} deformation band is present between 825 and 795 cm^{-1} [7]. Around 470 and 400 cm^{-1} the respective $Ln-O$ vibrations occur [23, 64]. A detailed assignment of the bands can be found in Table S5 (Supporting Information).

Table 5: Correlation scheme for D_{3h} , D_3 , C_{2v} , C_s for the CO_3^{2-} ion^a.

D_{3h}	D_3	C_{2v}	C_s
$A_1'(R)(\nu_1)$	—	$A_1'(I,R)(\nu_1)$	$A'(I,R)(\nu_1, 2\nu_3, 2\nu_4)$
$A_2''(I)(\nu_2)$	—	$B_1(I,R)(\nu_2)$	
$E'(I,R)(\nu_3, \nu_4)$	—	$A_1 + B_2(I,R)(2\nu_3, 2\nu_4)$	$A''(I,R)(\nu_2)$

^aI: infrared-active; R: Raman-active; ν_1 : symmetric C–O stretching; ν_2 : CO_3 out-of-plane deformation; ν_3 : asymmetric C–O stretching; ν_4 : CO_3 in-plane deformation mode.

2.6 UV/Vis spectroscopy

The optical properties of $La[CO_3][OH]$, $Pr[CO_3][OH]$, $Eu[CO_3][OH]$, and $Gd[CO_3][OH]$ have been determined by UV/Vis spectroscopy (Fig. 6). The spectra show the expected electronic transitions for Pr^{3+} and Eu^{3+} . The absorption maxima at 440, 448, 465, 485 and 580 nm correspond to the ${}^3H_4 \rightarrow {}^3P_2$, ${}^3H_4 \rightarrow {}^1I_6$, ${}^3H_4 \rightarrow {}^3P_1$, ${}^3H_4 \rightarrow {}^3P_0$ and ${}^3H_4 \rightarrow {}^1D_2$ transitions of Pr^{3+} , respectively [65]. The characteristic transitions for Eu^{3+} , ${}^7F_0 \rightarrow {}^5L_6$, ${}^7F_0 \rightarrow {}^5D_2$ and ${}^7F_0 \rightarrow {}^5D_1$, result in the reflexion minima at 395, 466 and 534 nm, respectively [66]. As expected, no such transitions are observed within the range of measurement for La^{3+} . Below 300 nm the fundamental absorption of the samples' band gaps governed by the carbonate ion is rising [67]. With increasing distance of the CO_3^{2-} from the rare earth ion (already discussed in Table 2) the onset of the absorption is shifted to lower wavelengths. The absorption below 300 nm overlaps the transitions for Gd^{3+} . Consequently, the ${}^8S_{7/2} \rightarrow {}^6I_{7/2}$ and ${}^8S_{7/2} \rightarrow {}^6P_{7/2}$ transitions expected at around 310 and 280 nm could not be observed [68].

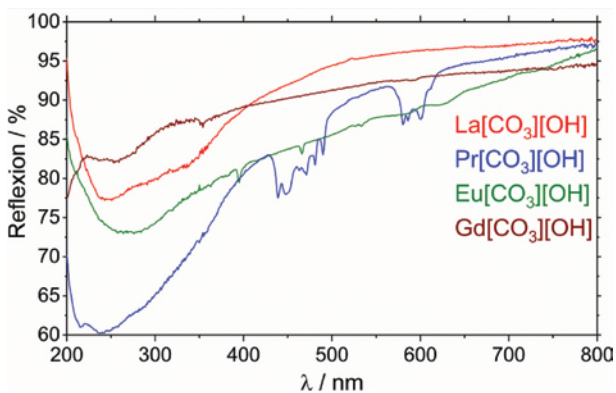
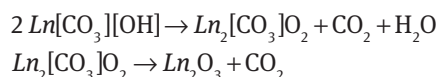


Fig. 6: UV/Vis spectra of $La[CO_3][OH]$, $Pr[CO_3][OH]$, $Eu[CO_3][OH]$ and $Gd[CO_3][OH]$.

2.7 Thermal analysis

The compounds $Ln[CO_3][OH]$ are well known as precursors for the preparation of $Ln_2[CO_3]O_2$ and Ln_2O_3 compounds. The thermolysis properties were investigated using thermal analysis. For all compounds, a two-step process was observed (See Fig. 7) following the reaction equations [11–15]



The DTG curves reveal the first reaction to take place around $T = 469, 449$ and $514^\circ C$ and the second step to occur around $T = 745, 685$ and $612^\circ C$ for $La[CO_3][OH]$, $Pr[CO_3][OH]$ and $Eu[CO_3][OH]$, respectively. The mass losses during these decompositions match well with the expected values

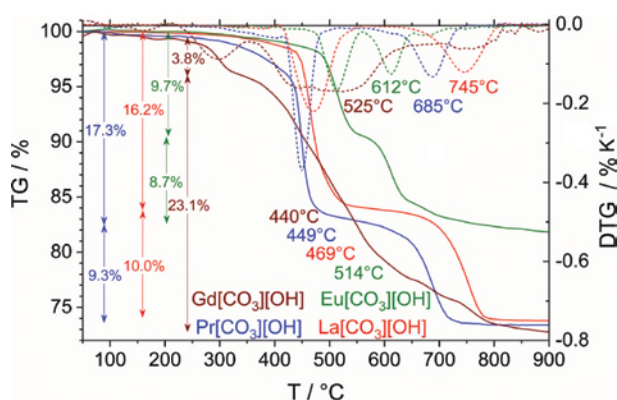


Fig. 7: Thermal analysis of $La[CO_3][OH]$, $Pr[CO_3][OH]$, $Eu[CO_3][OH]$, and $Gd[CO_3][OH]$: Both the mass loss (TG in %) and the first derivative of the mass loss with temperature (DTG in $\% K^{-1}$) are given.

from the reaction equation (Table S6; Supporting Information). The $La[CO_3][OH]$ sample lost 16.2 wt.-% during the first step compared to 14.4 wt.-% expected for the loss of one CO_2 and one H_2O molecule. For $Pr[CO_3][OH]$, the experimental value for the first step is also slightly higher due to residues decomposing at low temperature. Only for $Eu[CO_3][OH]$, the experimental value is lower than the theoretical one. This is presumably due to the post-synthesis heating step of the sample in order to remove side phases. A mass loss of 10 wt.-% was determined after this step explaining the deviation for the $Eu[CO_3][OH]$ sample which showed an experimental loss of 9.7 wt.-% compared to the expected 13.5 wt.-%. During this step the decomposition of $Eu[CO_3][OH]$ has already begun. For the second step, all samples match the expected values, e. g. a mass loss of 10.0 wt.-% is measured for $La[CO_3][OH]$ compared to 10.2 wt.-% expected. For $Gd[CO_3][OH]$, a non-heat-treated sample was used showing a mass loss of 3.8 wt.-% at $300^\circ C$ due to the decomposition of the side phases. The further decomposition steps appear to overlap each other. However, the overall mass loss of 23.1 wt.-% compared to expected 22.6 wt.-% fits to the decomposition of $Gd[CO_3][OH]$ to Gd_2O_3 . For all four samples, the phase transitions are confirmed by temperature dependent powder X-ray diffraction (Figs. S7–S10; Supporting Information).

Additional DSC measurements have supported the transition temperatures taken from the DTG curves with endothermic peaks at $T = 459, 456$ and $463^\circ C$ for $La[CO_3][OH]$, $Pr[CO_3][OH]$ and $Eu[CO_3][OH]$, respectively (Fig. S4; Supporting Information). The peaks represent the phase transformation from $Ln[CO_3][OH]$ to $Ln_2[CO_3]O_2$. Further, the DSC measurements of $Eu[CO_3][OH]$

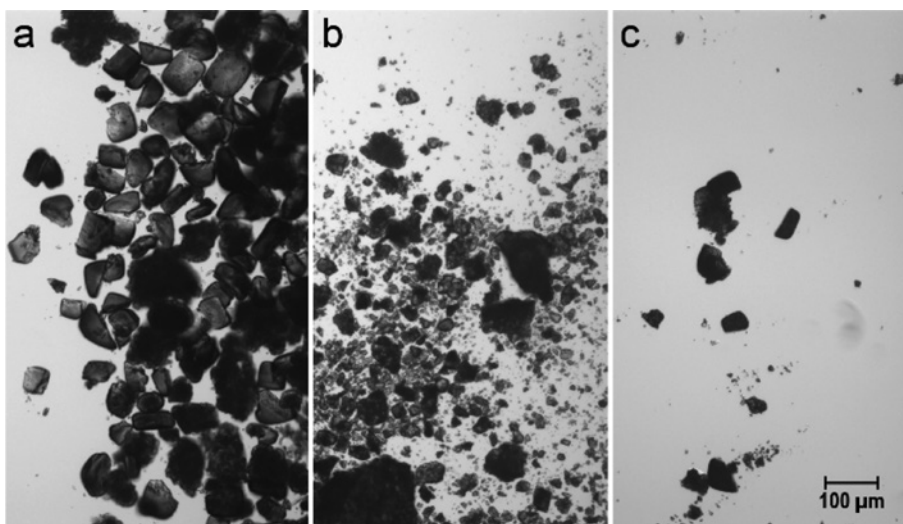


Fig. 8: Microscope pictures of (a) $Eu[CO_3][OH]$, (b) $Eu_2[CO_3]O_2$ and (c) Eu_2O_3 showing the inheritance of the morphology from the precursor during the decomposition.

and $Gd[CO_3][OH]$ revealed an extra endothermic peak at $T = 350^\circ C$ corresponding to the decomposition of the side phases, which is the reason for the need of an additional heat treatment. This peak is not present for $La[CO_3][OH]$ and $Pr[CO_3][OH]$.

Moreover, another requirement for the possible use of the compounds as precursors is the passing on of the morphology of the precursors to the final products. This behaviour could be observed for the presented compounds as can be seen in the microscope pictures in Figs. 8, S11 and S12 (Supporting Information). The $Ln[CO_3][OH]$ samples consist of single crystals and their shape is inherited by the polycrystalline $Ln_2[CO_3]O_2$ and Ln_2O_3 products accompanied by a size reduction due to the release of gaseous CO_2 and H_2O . Consequently, the hydrothermally synthesised $Ln[CO_3][OH]$ samples are suited for the use as precursors.

3 Conclusions

In this contribution, we obtained the compounds $Ln[CO_3][OH]$ ($Ln = La, Pr, Nd, Sm, Eu, Gd$) via hydrothermal syntheses using ambient CO_2 as carbonate source, thus resembling the natural formation of the minerals *ancylite* or *kozoite*. We also obtained single crystals of high quality allowing for the unequivocal localisation of hydrogen. There is no indication for the absence of an inversion centre in the crystal structures. This result has been confirmed by the powder SHG method which did not deliver any SHG intensity. We could therefore clarify the discussion ongoing in the literature regarding the proper space group assignment of $Pnma$ instead of $P2_12_1$. None of the previous investigations proved the absence of inversion symmetry by recording the non-linear optical properties. Moreover, our investigations have confirmed the chemically inspired assumption that the hydroxide form is favoured over the oxide hydrate form as the crystallographic surrounding of the non-carbonate oxygen atoms is very similar. Consequently, $Ln_2O(CO_3)_2 \cdot H_2O$ is apparently identical with $Ln[CO_3][OH]$.

We have further demonstrated the possible application of the carbonate hydrates as precursors for the corresponding carbonate oxides and the pure oxides.

4 Experimental section

4.1 Materials

$La(NO_3)_3 \cdot 6H_2O$, $Nd(NO_3)_3 \cdot 6H_2O$, $Pr(NO_3)_3 \cdot 6H_2O$, $Tb(NO_3)_3 \cdot 5H_2O$ (all from Strem Chemicals, Inc.),

$Eu(NO_3)_3 \cdot 5H_2O$, $Sm(NO_3)_3 \cdot 6H_2O$ (both from Alfa Aesar), $Gd(NO_3)_3 \cdot xH_2O$ (Chempur), $Ce(NO_3)_3 \cdot 5H_2O$ (Merck) and cetyltrimethylammonium bromide (Fluka) were used as starting materials without further purification and were handled in air.

4.2 Syntheses

A 1 mmol quantity of a rare earth nitrate hydrate and 0.5 mmol cetyltrimethylammonium bromide (CTAB) were dissolved in 20 mL H_2O . After stirring for 20 min at $70^\circ C$ the solution ($pH = 5$) was transferred into 30 mL PTFE pressure digestion vessels [69], which were heated in a compartment dryer at $180^\circ C$ for 5 days. After the vessels naturally cooled to room temperature, the precipitates were separated and washed by centrifugation at 4000 rpm for 10 min with deionised water three times and subsequently dried in a compartment dryer at $65^\circ C$ for 24 h.

Additionally, the $Nd[CO_3][OH]$, $Sm[CO_3][OH]$, $Eu[CO_3][OH]$, and $Gd[CO_3][OH]$ samples were heated in a corundum crucible for 10 h at $350^\circ C$ in air in order to decompose side phases with heating ramps of $200 K h^{-1}$.

4.3 Characterisation

4.3.1 X-ray structure determination

Suitable single crystals were selected for single-crystal XRD under a polarising microscope. Diffraction data were collected with a Bruker D8 Venture diffractometer using $MoK\alpha$ radiation ($\lambda = 0.7093 \text{ \AA}$). Absorption correction was performed by the multiscan method with the program SAINT within the Bruker APEX-II software suite. The structures were solved by Direct Methods and refined by full-matrix least-squares technique with the SHELXTL crystallographic software package [70]. The hydrogen atoms were refined using residual density of electrons for localisation and a reasonable restraint for the length of the O–H bond [63]. Relevant crystallographic data and further details of the structure determinations are summarised in Table 1.

Further details of the crystal structure investigations may be obtained from the Fachinformationszentrum Karlsruhe, 76344 Eggenstein-Leopoldshafen, Germany (Fax: +49-7247-808-666; E-Mail: crysdata@fiz-karlsruhe.de, <http://www.fiz-karlsruhe.de/request> for deposited data.html) on quoting the depository numbers CSD-1862162 ($LaCO_3OH$), CSD-1862163 ($PrCO_3OH$), CSD-1862164 ($EuCO_3OH$) and CSD-1862165 ($GdCO_3OH$).

4.3.2 X-ray powder diffraction

Ground samples were prepared on a stainless steel sample holder and flattened using a glass plate. The X-ray powder diffraction patterns were recorded with a Seifert 3003 TT diffractometer at room temperature in Bragg-Brentano geometry using $Cu-K\alpha$ radiation, a GE METEOR 1D line detector, and a Ni-Filter to suppress $K\beta$ radiation (X-ray tube operated at 40 kV and 40 mA, scan range: 5–80°, increment: 0.02°, 40 scans per data point, integration time: 200 s per degree).

4.3.3 Variable-temperature X-ray powder diffraction

The samples were ground and filled into a silica-glass Hilgenberg glass capillary (outer diameter 0.3 mm, wall thickness 0.01 mm). The data were collected between $T=50$ and 920°C with a Bruker D8 Advance diffractometer with $CuK\alpha$ radiation ($\lambda = 1.54184 \text{ \AA}$) with a 1D LynxEye detector, steps of 0.02°, acquisition time 3 s per step and transmission geometry. The generator operated at 38 kV and 40 mA.

4.3.4 EDX/SEM

The elemental composition of solid $Ln[CO_3][OH]$ ($Ln = La, Pr, Eu, Gd$) samples was determined by energy dispersive X-ray spectroscopy (EDX) with a Philips XL 30 FEG scanning electron microscope (SEM) equipped with an EDAX SiLi detector.

4.3.5 FTIR spectroscopy

The Fourier-transform infrared spectra were recorded at room temperature with a Bruker EQUINOX 55 T-R spectrometer using a Platinum ATR device (scan range: 400–4000 cm^{-1} , resolution: 4 cm^{-1} , 32 scans per sample).

4.3.6 UV/Vis spectroscopy

The UV/Vis spectra were recorded as diffuse reflection spectra at room temperature with a Varian Cary 300 Scan UV/Vis spectrophotometer using an Ulbricht sphere detector and a deuterium lamp / mercury lamp light source (scan range: 200–800 nm, increment 1 nm, scan rate: 120 $nm \cdot min^{-1}$).

4.3.7 SHG measurement

The powder SHG method developed by Kurtz and Perry [50] is commonly used in the first step to estimate the non-linear optical properties of new materials or to detect the absence of an inversion centre in crystalline structures [49]. A Q-switched Nd:YAG laser (Impex-hightech, 1064-Q-HP, 2kHz), operating at 1064 nm and a pulse width of 5 ns provided the fundamental wave. With a harmonic separator, a short-pass filter, and interference filter, the fundamental infrared light was separated from the generated second harmonic. The generated SHG signal at 532 nm was collected using a photomultiplier (R2949, Hamamatsu) and an oscilloscope (Tektronix). The average values of different areas are presented here. SHG signals from five different areas of the sample were measured to check the homogeneity of the sample. The measured intensities were corrected by subtracting a background signals collected between the pulses.

4.3.8 Thermogravimetry

The TG analyses were performed with a NETZSCH STA 409 PC Luxx thermobalance under N_2 atmosphere with 70 $mL \cdot min^{-1}$ flow in alumina crucibles (heating rate: 10 $K \cdot min^{-1}$). Besides standard TG, differential thermogravimetry, e.g. the first derivative of the mass loss with respect to temperature was investigated.

4.3.9 Differential scanning calorimetry

The DSC measurements were undertaken on a TA Instruments DSC 2920 in a 50 $mL \cdot min^{-1}$ N_2 flow using Netzsch standard Al pans with pierced lids with a heating rate of 5 $K \cdot min^{-1}$.

4.3.10 Microscopy

The synthesis products, the products of the TG analyses of $La[CO_3][OH]$, $Pr[CO_3][OH]$ and $Eu[CO_3][OH]$ and samples of $La[CO_3][OH]$, $Pr[CO_3][OH]$ and $Eu[CO_3][OH]$ heated in corundum crucibles for 10 h at $T=470, 460$ and 500°C, respectively were investigated by light microscopy. These temperatures correspond to the maxima in the DTG curves related to the transformation into $Ln_2[CO_3]O_2$. The heating ramps were 200 $K \cdot h^{-1}$. An Olympus IX70 Microscope with a Abrio CRi CCD camera was used.

5 Supporting information

Supporting data associated with this article can be found as supplementary material available online (DOI: 10.1515/znb-2018-0170).

Acknowledgements: The authors would like to thank R. Ettliger (Universität Augsburg) for the EDX/SEM measurements and L. Bayarjargal (Universität Frankfurt) for testing our powder samples for non-linear optical SHG activity.

References

- [1] S. G. Jantz, M. Dialer, L. Bayarjargal, B. Winkler, L. van Wüllen, F. Pielhofer, J. Brgoch, R. Wehrich, H. A. Höppe, *Adv. Opt. Mater.* **2018**, *7*, 1800497.
- [2] S. G. Jantz, F. Pielhofer, M. Dialer, H. A. Höppe, *Z. Anorg. Allg. Chem.* **2017**, *643*, 2024.
- [3] S. G. Jantz, F. Pielhofer, M. Dialer, H. A. Höppe, *Z. Anorg. Allg. Chem.* **2017**, *643*, 2031.
- [4] S. G. Jantz, F. Pielhofer, L. van Wüllen, R. Wehrich, M. J. Schäfer, H. A. Höppe, *Chem. Eur. J.* **2018**, *24*, 443.
- [5] P. Netzsch, P. Gross, H. Takahashi, H. A. Höppe, *Inorg. Chem.* **2018**, *57*, 8530.
- [6] A. M. Kaczmarek, L. Miermans, R. van Deun, *Dalton Trans.* **2013**, *42*, 4639.
- [7] M.-H. Lee, W.-S. Jung, *Bull. Kor. Chem. Soc.* **2013**, *34*, 3609.
- [8] B. Pan, Q. Xie, H. Wang, J. Zhu, Y. Zhang, W. Su, X. Wang, *J. Mater. Chem. A* **2013**, *1*, 6629.
- [9] Y.-C. Chen, L. Qin, Z.-S. Meng, D.-F. Yang, C. Wu, Z. Fu, Y.-Z. Zheng, J.-L. Liu, R. Tarasenko, M. Orendáč, J. Prokleška, V. Sechovský, M.-L. Tong, *J. Mater. Chem. A* **2014**, *2*, 9851.
- [10] J. M. Calderon Moreno, V. G. Pol, S.-H. Suh, M. Popa, *Inorg. Chem.* **2010**, *49*, 10067.
- [11] L. M. D'Assunção, I. Giolito, M. Ionashiro, *Thermochim. Acta* **1989**, *137*, 319.
- [12] P. Jeevanandam, Y. Koltypin, O. Palchik, A. Gedanken, *J. Mater. Chem.* **2001**, *11*, 869.
- [13] A. M. Kaczmarek, K. van Hecke, R. van Deun, *Chem. Soc. Rev.* **2015**, *44*, 2032.
- [14] Z. Xu, S. Bian, J. Wang, T. Liu, L. Wang, Y. Gao, *RSC Adv* **2013**, *3*, 1410.
- [15] Y. Zhang, Z. Xu, X. Yin, Z. Fang, W. Zhu, H. He, *Cryst. Res. Technol.* **2010**, *45*, 1183.
- [16] L. Bischoff, M. Stephan, C. S. Birkel, C. F. Litterscheid, A. Dreizler, B. Albert, *Sci. Rep.* **2018**, *8*, 602.
- [17] S. Huang, D. Wang, Y. Wang, L. Wang, X. Zhang, P. Yang, *J. Alloys Compd.* **2012**, *529*, 140.
- [18] Y. Zhang, L. Jin, K. Sterling, Z. Luo, T. Jiang, R. Miao, C. Guild, S. L. Suib, *Green Chem.* **2015**, *17*, 3600.
- [19] G. Mao, H. Zhang, H. Li, J. Jin, S. Niu, *J. Electrochem. Soc.* **2012**, *159*, J48.
- [20] I. Nelli, A. M. Kaczmarek, F. Locardi, V. Caratto, G. A. Costa, R. van Deun, *Dalton Trans.* **2017**, *46*, 2785.
- [21] H. A. Höppe, G. Kotzyba, R. Pöttgen, W. Schnick, *J. Solid State Chem.* **2002**, *167*, 393.
- [22] H. A. Höppe, *Angew. Chem. Int. Ed.* **2009**, *48*, 3572.
- [23] C. S. Riccardi, R. C. Lima, M. L. dos Santos, P. R. Bueno, J. A. Varela, E. Longo, *Solid State Ionics* **2009**, *180*, 288.
- [24] T. Tahara, I. Nakai, R. Miyawaki, S. Matsubara, *Z. Kristallogr.* **2007**, *222*, 326.
- [25] A. N. Christensen, G. Sundström, C. A. Wachtmeister, J. Songstad, A. H. Norbury, C.-G. Swahn, *Acta Chem. Scand.* **1973**, *27*, 2973.
- [26] T. Doert, O. Rademacher, J. Getzschmann, *Z. Kristallogr. – NCS* **1999**, *214*, 11.
- [27] K. Michiba, T. Tahara, I. Nakai, R. Miyawaki, S. Matsubara, *Z. Kristallogr.* **2011**, *226*, 314.
- [28] C. Heinrichs, *Synthese und Charakterisierung wasserfreier Seltenerdmetall-Nitrate, -Acetate und -Oxyacetate*, Dissertation, Universität zu Köln, Köln, **2013**.
- [29] G. W. Beall, W. O. Milligan, S. Mroczkowski, *Acta Crystallogr. B* **1976**, *32*, 3143.
- [30] H.-S. Sheu, W.-J. Shih, W.-T. Chuang, I.-F. Li, C.-S. Yeh, *J. Chin. Chem. Soc.* **2010**, *57*, 938.
- [31] Y. Zhang, K. Han, X. Yin, Z. Fang, Z. Xu, W. Zhu, *J. Crystal Growth* **2009**, *311*, 3883.
- [32] Z. Li, J. Zhang, J. Du, H. Gao, Y. Gao, T. Mu, B. Han, *Mater. Lett.* **2005**, *59*, 963.
- [33] A. dal Negro, G. Rossi, V. Tazzoli, *Am. Mineral.* **1975**, *60*, 280.
- [34] R. Miyawaki, S. Matsubara, K. Yokoyama, S. Iwano, K. Hama-saki, I. Yukinori, *J. Miner. Petr. Sci.* **2003**, *98*, 137.
- [35] R. Miyawaki, S. Matsubara, K. Yokoyama, K. Takeuchi, Y. Terada, I. Nakai, *Am. Mineral.* **2000**, *85*, 1076.
- [36] P. Orlandi, M. Pasero, G. Vezzalini, *Eur. J. Miner.* **1990**, *2*, 413.
- [37] J. P. Attfield, G. Férey, *J. Solid State Chem.* **1989**, *82*, 132.
- [38] A. Olafsen, A.-K. Larsson, H. Fjellvåg, B. C. Hauback, *J. Solid State Chem.* **2001**, *158*, 14.
- [39] I. Kutlu, G. Meyer, *Z. Anorg. Allg. Chem.* **1999**, *625*, 402.
- [40] A. N. Christensen, S. E. Rasmussen, E. Kvamme, R. Ohlson, A. Shimizu, *Acta Chem. Scand.* **1970**, *24*, 2440.
- [41] T. Zhang, G. Xu, J. Puckette, F. D. Blum, *J. Phys. Chem. C* **2012**, *116*, 11626.
- [42] C. Pan, D. Zhang, L. Shi, *J. Solid State Chem.* **2008**, *181*, 1298.
- [43] P. Schmidt, *Thermodynamische Analyse der Existenzbereiche fester Phasen – Prinzipien der Synthesepaltung in der anorganischen Festkörperchemie, Habilitationsschrift*, Technische Universität Dresden, Dresden, **2007**.
- [44] R. D. Shannon, *Acta Cryst A* **1976**, *32*, 751.
- [45] S. A. Morozov, *Russ. J. Gen. Chem.* **2003**, *73*, 37.
- [46] F. A. Andersen, L. Brečević, G. Beuter, D. B. Dell'Amico, F. Calderazzo, N. J. Bjerrum, A. E. Underhill, *Acta Chem. Scand.* **1991**, *45*, 1018.
- [47] K. Nakamoto, *Infrared and Raman Spectra of Inorganic and Coordination Compounds*, 6th edition, Wiley-Blackwell, Oxford, **2008**.
- [48] A. L. Spek, *Acta Crystallogr.* **2009**, *D65*, 148.
- [49] J. P. Dougherty, S. K. Kurtz, *J. Appl. Crystallogr.* **1976**, *9*, 145.
- [50] S. K. Kurtz, T. T. Perry, *J. Appl. Phys.* **1968**, *39*, 3798.
- [51] V. Petříček, M. Dušek, L. Palatinus, *Z. Kristallogr.* **2014**, *229*, 345.
- [52] H. A. Höppe, *Z. Naturforsch.* **2015**, *70b*, 769.
- [53] R. Hoppe, *Angew. Chem.* **1966**, *78*, 52.
- [54] R. Hoppe, *Angew. Chem. Int. Ed. Engl.* **1970**, *9*, 25.

- [55] R. Hübenthal, MAPLE, Program for the Calculation of the Madelung Part of Lattice Energy, Universität Gießen, Gießen (Germany), **1993**.
- [56] G. Schiller, *Die Kristallstrukturen von Ce_2O_3 (A-Form), $LiCeO_2$ und CeF_3 – Ein Beitrag zur Kristallchemie des dreiwertigen Cers*, Dissertation, Universität Karlsruhe, Karlsruhe, **1985**.
- [57] A. Goto, T. Hondoh, S. Mae, *J. Chem. Phys.* **1990**, *93*, 1412.
- [58] T. Pilati, F. Demartin, C. M. Gramaccioli, *Acta Crystallogr.* **1998**, *A54*, 515.
- [59] I. Oftedal, *Z. Phys. Chem.* **1927**, *128U*, 154.
- [60] H. C. R. Wolf, R. Hoppe, *Z. Anorg. Allg. Chem.* **1985**, *529*, 61.
- [61] A. Saiki, N. Ishizawa, N. Mizutani, M. Kato, *J. Ceram. Assoc. Jpn.* **1985**, *93*, 649.
- [62] S. A. Mohitkar, J. Nuss, H. A. Höppe, C. Felser, M. Jansen, *Dalton Trans.* **2018**, *47*, 5968.
- [63] T. Steiner, *Angew. Chem. Int. Ed.* **2002**, *41*, 48.
- [64] N. T. McDevitt, W. L. Baun, *Spectrochim. Acta* **1964**, *20*, 799.
- [65] W. T. Carnall, P. R. Fields, K. Rajnak, *J. Chem. Phys.* **1968**, *49*, 4424.
- [66] W. T. Carnall, P. R. Fields, K. Rajnak, *J. Chem. Phys.* **1968**, *49*, 4450.
- [67] S. Ni, T. Li, X. Yang, *J. Alloys Compd.* **2011**, *509*, 7874.
- [68] W. T. Carnall, P. R. Fields, K. Rajnak, *J. Chem. Phys.* **1968**, *49*, 4412.
- [69] H. Heinrichs, H.-J. Brumsack, N. Loftfield, N. König, *Z. Pflanzenernähr. Bodenkd.* **1986**, *149*, 350.
- [70] G. M. Sheldrick, *Acta Crystallogr.* **2015**, *C71*, 3.

Supplementary Material: The online version of this article offers supplementary material (<https://doi.org/10.1515/znb-2018-0170>).